www.nature.com/aps

Acta Pharmacologica Sinica

ARTICLE

Pan-KRAS inhibitors suppress proliferation through feedback regulation in pancreatic ductal adenocarcinoma

Cheng-xiang Wang[1], Ting-ting Wang[2], Kun-dong Zhang[3], Ming-yu Li[1], Qian-cheng Shen[2], Shao-yong Lu[1,2] and Jian Zhang[1,2,4]

Pancreatic ductal adenocarcinoma (PDAC) is currently one of the most lethal cancers worldwide. Several basic studies have confirmed that Kirsten rat sarcoma virus (*KRAS*) is a key driver gene for the occurrence of PDAC, and *KRAS* mutations have also been found in most patients in clinical studies. In this study, two pan-KRAS inhibitors, BI-2852 and BAY-293, were chosen as chemical probes to investigate their antitumor potency in PDAC. Their inhibitory effects on KRAS activation were validated in vitro and their antiproliferative potency in PDAC cell lines were profiled, with half-maximal inhibitory concentration (IC_{50}) values of approximately 1 μM, demonstrating the therapeutic potential of pan-KRAS inhibitors in the treatment of PDAC. However, feedback regulation in the KRAS pathway weakened inhibitor activity, which was observed by a 50 times difference in BAY-293 from in vitro activity. Furthermore, pan-KRAS inhibitors effectively inhibited cell proliferation in 3D organoids cultured from PDAC patient samples; however, there were some variations between individuals. These results provide a sufficient theoretical foundation for KRAS as a clinical therapeutic target and for the application of pan-KRAS inhibitors in the treatment of PDAC, with important scientific significance in translational medicine.

Keywords: pancreatic ductal adenocarcinoma; KRAS; driver gene; BAY-293; organoid

Acta Pharmacologica Sinica (2022) 43:2696–2708; https://doi.org/10.1038/s41401-022-00897-4

INTRODUCTION

Pancreatic cancer (PC) is a heavy disease burden worldwide [1, 2]. In 2021 [3], PC was the fourth leading cause of cancer-related deaths. The 5-year survival rate for PC is 10%, which is the lowest among all cancer types [3]. Pancreatic ductal adenocarcinoma (PDAC) is the most malignant type of PC. Most patients with pancreatic cancer are diagnosed at an advanced stage, which greatly limits the possibility of surgical treatment [4]. Chemotherapy and radiotherapy are currently the major clinical treatment options of PDAC [5]. Gemcitabine is the first-line drug against PDAC; however, resistance develops within weeks of chemotherapy initiation [6, 7]. Therefore, there is an urgent need to develop new therapies to treat PDAC. Many basic studies have found that Kirsten rat sarcoma virus (*KRAS*) is a key driver gene for the occurrence of PDAC [8], and *KRAS* mutations have also been found in most patients in clinical studies [9, 10]. Furthermore, mutant *KRAS* is strongly associated with invasion and poor prognosis of PDAC [11, 12].

KRAS is a member of the rat sarcoma virus (RAS) family, which includes *KRAS*, neuroblastoma RAS (*NRAS*), and Harvey RAS (*HRAS*). KRAS oncoprotein is a small guanosine triphosphatase (GTPase) that regulates signaling pathways as a molecular switch cycling between an active guanosine triphosphate (GTP)-bound state and an inactive guanosine diphosphate (GDP)-bound state [13, 14]. KRAS is activated by guanine nucleotide exchange factors (GEFs) and interacts with effector proteins to activate downstream signaling pathways, thus regulating cell growth, survival, and proliferation. GTPase-activated proteins (GAPs) promote GTP hydrolysis of KRAS and return KRAS to an inactive state [15–17]. Oncogenic KRAS mutations frequently occur in codons 12, 13, and 61, which disrupt GAP-mediated GTP hydrolysis, keeping KRAS in its active state that persists to activate downstream signaling pathways [18, 19]. *KRAS* is a tumor driver gene in many cancers, including PDAC, colorectal cancer (CRC), and lung adenocarcinoma (LUAD), a subtype of non-small cell lung cancer (NSCLC) [20]. Activating *KRAS* mutations are found in approximately 90% of PDAC patients, supporting that they are key targets for PDAC treatment [21].

Although targeting KRAS has great benefits, it is difficult to specifically target. Recently, AMG 510, a covalent KRAS G12C inhibitor, was approved by the FDA for the treatment of NSCLC harboring the $KRAS^{G12C}$ mutation [22]. Thus, targeting the *KRAS* mutation allele is an efficient and promising therapeutic strategy for *KRAS*-driven tumors. However, there are more prevalent KRAS mutation alleles in PDAC, including G12D, G12V, and G12R, which lack the targeted compounds. It is challenging to develop specific compounds that target each KRAS mutation allele. PDAC is a complex and multi-gene mutational cancer with obvious tumor heterogeneity [23]. Pan-KRAS inhibitors may serve as a promising treatment for PDAC, targeting all types of KRAS mutations without

[1]State Key Laboratory of Oncogenes and Related Genes, Key Laboratory of Cell Differentiation and Apoptosis of Chinese Ministry of Education, Shanghai Jiao Tong University, School of Medicine, Shanghai 200025, China; [2]Medicinal Chemistry and Bioinformatics Center, Shanghai Jiao Tong University, School of Medicine, Shanghai 200025, China; [3]Department of General Surgery, Shanghai General Hospital, Shanghai Jiao Tong University, Shanghai 200080, China and [4]School of Pharmaceutical Sciences, Zhengzhou University, Zhengzhou 450001, China
Correspondence: Shao-yong Lu (lushaoyong@sjtu.edu.cn) or Jian Zhang (jian.zhang@sjtu.edu.cn)
These authors contributed equally: Cheng-xiang Wang, Ting-ting Wang and Kun-dong Zhang

Received: 2 November 2021 Accepted: 6 March 2022
Published online: 29 March 2022

any KRAS mutation allele enrichment after treatment. In 2019, two pan-KRAS inhibitors, BI-2852 [24] and BAY-293 [25], were reported to inhibit the activation of KRAS by SOS1 and the proliferation of lung cancer cells.

The present study focused on two pan-KRAS inhibitors, BI-2852 and BAY-293, as pharmacological tools to investigate whether targeting KRAS had anti-PDAC activity. It was found that BI-2852 and BAY-293 effectively inhibited the proliferation of PDAC cell lines by blocking KRAS activation and downregulating the phosphorylation of downstream effectors. However, there was feedback regulation that impaired the activity of compounds in cancer cells, which was further shown by Western blotting and RNA sequencing (RNA-Seq). Furthermore, BAY-293 induced apoptosis in MIA PaCa-2 cells, but not in PANC-1 cells. BAY-293 showed promising therapeutic potential in patient-derived organoids with individual patient variations. Collectively, the data obtained in this study provide evidence that pan-KRAS inhibitors may be a viable therapeutic strategy for PDAC.

MATERIALS AND METHODS

PDAC patient samples

Eleven PDAC patient samples were collected from 11 patients undergoing surgery at the Shanghai General Hospital Department of General Surgery, Shanghai Jiao Tong University. This study was approved by the Ethics Committee of Shanghai General Hospital, Shanghai Jiao Tong University. Informed written consent was obtained from all patients.

Chemical reagents

BI-2852 and BAY-293 were purchased from CSNpharm (Arlington Heights, USA), dissolved in 100% dimethyl sulfoxide (DMSO) to a stock concentration of 100 mM, and stored at −20 °C.

Construction of plasmids

The pET42a-KRAS4B (1-169) plasmid was a gift from Vadim Gaponenk with an N-terminal 6x histidine tag to facilitate protein purification [26]. The SOS1 (564-1049) gene was synthesized by Tsingke Biological Technology (Beijing, China) and cloned into the pET28a vector using *Nde*I and *Bam*HI restriction sites, an N-terminal 6x histidine tag was added to ease protein purification. Point mutations (G12C, G12D, and G12V) were introduced into the plasmid encoding KRAS4B (1-169) using the Mut Express II Fast Mutagenesis Kit V2 (Vazyme Biotech Co. Ltd., Nanjing, Jiangsu, China). Successful introduction of mutations was verified through DNA sequencing (Personalbio, Shanghai, China).

Expression and purification of proteins

The plasmid was transformed into *Escherichia coli* Rosetta (DE3) cells (Weidi, Shanghai, China) for protein purification. Cells were induced with 0.5 mM isopropyl β-*D*-1-thiogalactopyranoside (IPTG) (Sigma-Aldrich, St. Louis, USA) at 18 °C. KRAS protein was first purified using a nickel column (GE healthcare, Little Chalfont, UK) in lysis buffer (50 mM HEPES, pH 7.4, 500 mM NaCl, 2 mM $MgCl_2$, and 20 mM imidazole), and 1 mM dithiothreitol (DTT) (Sigma-Aldrich, St. Louis, USA) and protein inhibitor cocktail (ApexBio, Houston, USA) was added before French Press. Gel filtration chromatography was performed using a Superdex 75 column 10/300 GL (GE healthcare, Little Chalfont, UK) with buffer (50 mM Tris-citrate, pH 6.5; 50 mM NaCl; 5 mM $MgCl_2$; and 0.01 mM guanosine diphosphate [Sigma-Aldrich, St. Louis, USA] and 1 mM DTT). The mutated forms of KRAS protein were purified analogously. The SOS1 protein was purified using a nickel column (GE Healthcare, Little Chalfont, UK) in lysis buffer (25 mM Tris-HCl, pH 7.5; 500 mM NaCl; and 20 mM imidazole) and a protein inhibitor cocktail was added before French Press, eluted with 25 mM Tris-HCl, pH 7.5; 500 mM NaCl; and 250 mM imidazole. The SOS1 protein was then exchanged with storage buffer (25 mM Tris-HCl, pH 7.5; 50 mM NaCl; and 1 mM DTT).

Nucleotide exchange assay

KRAS protein was loaded with 20-fold fluorescent nucleotide analog N-methylanthraniloyl (MANT)-GDP (Invitrogen, Carlsbad, USA) in buffer containing 20 mM Tris-HCl, pH 7.5; 50 mM NaCl; 0.5 mM $MgCl_2$; 5 mM EDTA; and 1 mM DTT for 90 min at 20 °C to avoid light, as described previously [27]. Nucleotide loading was quenched by adding 10 mM $MgCl_2$ for 30 min at 20 °C. Free nucleotides were removed using a PD miniTrap column (GE Healthcare, Little Chalfont, UK), which was pre-equilibrated with reaction buffer (40 mM HEPES-KOH, pH 7.5; 10 mM $MgCl_2$; and 1 mM DTT). The nucleotide exchange assay medium contained 40 mM HEPES-KOH, pH 7.5; 10 mM $MgCl_2$; 1 mM DTT; 1 μM $KRAS^{MANT\text{-}GDP}$; 325 nM SOS1; 200 μM guanosine triphosphate (GTP) (Sigma-Aldrich, St. Louis, USA); and DMSO or compounds. Fluorescence was monitored using a Synergy Neo multimode microplate reader (Biotek, Winooski, USA), with excitation at $\lambda = 360$ nm and emission at $\lambda = 440$ nm every 1 min for 30 min at room temperature. The half-life inhibitory concentration (IC_{50}) values were calculated by fitting the data points with the dose-response function in GraphPad Prism version 7.0 (La Jolla, CA, USA).

Cell culture

All cancer cell lines (PDAC, NSCLC, and CRC) were obtained from the Stem Cell Bank of the Chinese Academy of Sciences. The Colo 320DM, Colo 201, Colo 205, AsPC-1, NCI-H460, DLD-1, HCT-15, HCT-8, BxPC-3, NCI-H358, NCI-H23, NCI-H1792, NCI-H1299, NCI-H1650, PC-9, HCC827, NCI-H520, and NCI-H292 cell lines were maintained in Roswell Park Memorial Institute (RPMI)-1640 medium supplemented with 10% (*v*/*v*) fetal bovine serum (FBS) (Gibco, Grand Island, USA). HCT 116, HT-29, and Calu-1 cell lines were maintained in McCoy's 5 A medium supplemented with 10% (*v*/*v*) FBS (Gibco, Grand Island, NY, USA). SW480, SW 1990, SW620, SW1417, and SW48 cell lines were maintained in L-15 medium supplemented with 10% (v/v) FBS (Gibco, Grand Island, USA). The RKO, LS 174 T, PANC-1, and MIA PaCa-2 cell lines were maintained in Dulbecco's Modified Eagle Medium (DMEM) supplemented with 10% (*v*/*v*) FBS (Gibco, Grand Island, USA). LoVo and A549 cell lines were maintained in F-12K medium supplemented with 10% (*v*/*v*) FBS (Gibco, Grand Island, USA). All cell lines were cultured according to the standard instructions provided by the American Type Culture Collection (ATCC). The cell lines were authenticated using short tandem repeat profiling.

Cell viability assay

In 3D spheroid culture, cells were seeded into ultra-low attachment 96-well plates (Corning #7007, Corning, USA) at a density of 1,500 cells per well and allowed to recover overnight in the culture medium. BI-2852 or BAY-293 were added at increasing concentrations, and DMSO treatment was used as a positive control. After 6 days of treatment, the number of living cells was measured by the addition of alamarBlue (Invitrogen, Carlsbad, USA). The relative viability of each group was presented as the percentage change relative to the positive control group and then fit to log (inhibitor) vs. normalized response curves using GraphPad Prism version 7.0 (La Jolla, USA).

For the patient-derived organoid (PDO) cell viability assay, 8 μL of Matrigel (Corning #354230, Corning, USA) was dispensed into 384-well plates. Cells were digested with TrypLE (Gibco, Grand Island, USA) and seeded into pre-coated 384-well plates, with 2%–5% Matrigel/grow media (15–20,000 organoids/mL) as previously described [28]. BAY-293 cells were added on the day after seeding. Cell viability was analyzed using alamarBlue after 6 days of incubation. The relative viability of each group was presented as the percentage change relative to the positive control (DMSO) group.

CFSE cell proliferation assay

Cells were seeded in six-well plates and allowed to attach overnight in DMEM containing 2% or 10% FBS. The CFSE reagent was dissolved in DMSO to a 5 mM storage concentration, and the CFSE stock solution was diluted in pre-warmed (37 °C) phosphate-buffered saline (PBS) to a working concentration of 5 μM. The culture medium was removed from the cells and replaced with working solution. The cells were then incubated for 20 min at 37 °C. The working solution was removed, and the cells were washed twice with culture medium containing 1% bovine serum albumin (BSA) and replaced with fresh, pre-warmed culture medium. The cells were incubated for 30 min at 37 °C to allow CFSE to undergo acetate hydrolysis. The control group was digested with trypsin and analyzed by flow cytometry and FlowJo software (Version 10; TreeStar, USA) after incubation, whereas the other groups were treated with DMSO or BAY-293 and analyzed after 4 days (MIA PaCa-2) or 5 days (PANC-1). Data were acquired using CytoFLEX S (Beckman Coulter, Brea, CA, USA).

Immunoblotting

Cells (2×10^5–3×10^5) were seeded in six-well plates and allowed to attach overnight. The cells were treated with DMSO or BAY-293. Cells were harvested at 1, 3, 6, 24, 48, and 72 h and lysed using RIPA lysis buffer (High) (EpiZyme, Shanghai, China). After BCA protein quantification (EpiZyme, Shanghai, China), the samples were added to 5 × SDS loading buffer and loaded into 4%–20% SurePAGE™ gels (Genscript, Jiangsu, China). The sample was transferred to 0.22 μm PVDF membranes (Millipore, Billerica, USA), blocked with 5% BSA in 1 × TBST for 1 h at room temperature, followed by incubation with specific primary antibodies overnight at 4 °C, and then with HRP-conjugated anti-rabbit immunoglobulin (Ig)G (#LF102, EpiZyme, Shanghai, China) or anti-mouse IgG (#LF101, EpiZyme, Shanghai, China) for 1 h at room temperature. Immunoreactive bands were visualized with a Biomolecular Imager (GE Healthcare, Little Chalfont, UK) using an ECL kit (EpiZyme, Shanghai, China).

RNA extraction and RNA-Seq analysis

Total RNA was extracted from MIA PaCa-2 and PANC-1 cells using TRIzol reagent (Beyotime, Shanghai, China), according to the manufacturer's instructions. Total RNA was sent to Tiangen (Beijing, China) for RNA sequencing using an Illumina Novaseq-6000 (Illumina, San Diego, USA). RNA-seq analysis was performed using the OmicShare tool, a free online platform for data analysis (https://www.omicshare.com/tools).

Cell apoptosis analysis

Cells (1×10^5) were seeded into six-well plates and allowed to attach overnight. The cells were treated with DMSO or BAY-293. After 48 h of treatment, cells were harvested using trypsin (0.25%) without EDTA (Gibco, Grand Island, NY, USA), followed by staining with Annexin V-APC and propidium iodide (PI) (eBiosciences, San Diego, CA, USA) according to the manufacturer's instructions. Samples were analyzed using flow cytometry and FlowJo software.

Patient-derived organoids culture

Patient tissue samples were minced and digested with collagenase II (5 mg/mL; Gibco, Grand Island, USA) in HBSS (Gibco, Grand Island, USA) at 37 °C for 2 h. Cells were harvested by passing through 100 μm sterile cell strainer (Miltenyi, Bergisch Gladbach, Germany) and centrifuged at 300 × *g* for 7 min. The primary cells were embedded in GFR Matrigel and cultured in PDAC complete medium (Advanced DMEM/F12 medium [Gibco, Grand Island, USA] supplemented with HEPES [1×, Gibco, Grand Island, USA], Glutamax [1×, Gibco, Grand Island, USA], B27 [1×, Gibco, Grand Island, USA], Primocin [1×, InvivoGen, San Diego, USA], *N*-acetyl-*L*-cysteine [1 mM, Sigma-Aldrich, St. Louis, USA], Wnt3a-conditioned medium [50% *v/v*], RSPO1-conditioned medium [10% *v/v*], Noggin-conditioned medium [10% *v/v*], epidermal growth factor [EGF, 50 ng/mL, Peprotech, Rocky Hill, USA], Gastrin [10 nM, CSNpharm, Arlington Heights, USA], fibroblast growth factor 10 [FGF10, 100 ng/mL, Preprotech, Rocky Hill, USA], Nicotinamide [10 mM, Sigma-Aldrich, St. Louis, USA], and A83-01 [0.5 mM, CSNpharm, Arlington Heights, USA]) [29].

Histological and immunohistochemical (IHC) analyses

Patient tissue samples and PDOs were fixed in 4% paraformaldehyde at 4 °C, embedded in paraffin, and sectioned using a semi-automated rotary microtome (Leica, Wetzlar, Germany). Sections were subjected to H&E and immunohistochemical staining using standard protocols. The anti-Ki-67 (1:300 dilution, ab15580, Abcam, Cambridge, MA, USA), anti-CK19 (1:300 dilution, 4558 T, CST, Danvers, MA, USA), and anti-SOX9 (1:600 dilution, 82630 T, CST) primary antibodies were used for immunohistochemical staining. Images were captured using a Pannoramic DESK P-MIDI slide scanner (3D HISTECH, Hungary).

DNA extraction and *KRAS* genotype identification of patient samples

The DNA of the patient samples was extracted using a DNA extraction kit (AmoyDX, Fujian, China), according to the manufacturer's instructions. Identification was performed using a human *KRAS* gene mutation detection kit (AmoyDX, Fujian, China) according to the manufacturer's instructions on Mx3000P real-time PCR equipment (Agilent Technologies, Santa Clara, CA, USA).

Statistical analysis

All data were analyzed using Microsoft Office Excel 2016 and GraphPad Prism Version 7.0, and are shown as the mean ± SD error of independent biological experiments, unless stated otherwise. Statistical analysis was performed using two-tailed Student's *t*-test or analysis of variance (ANOVA), unless stated otherwise. Statistical significance was set at $P < 0.05$ at groups ($^*P < 0.05$, $^{**}P < 0.01$, and $^{***}P < 0.001$). All investigators were blinded to each experiment.

RESULTS

BI-2852 and BAY-293 inhibited the activation of KRAS mediated by SOS1

KRAS is a small GTPase cycle between a GTP-bound active state and GDP-bound inactive state [16]. Interrupting the activation of KRAS mediated by GEFs blocks downstream signaling pathways, resulting in the suppression of cancer cell proliferation [30, 31]. BI-2853 and BAY-293 have been reported to serve as pan-KRAS inhibitors disrupting the interaction between KRAS and SOS1, the key GEF for KRAS [24, 25]. These two pan-KRAS inhibitors were used as pharmacological probes to investigate the potential therapeutic effects of targeting KRAS in the treatment of PDAC. The chemical structures of the two compounds are shown in Fig. 1a. Nucleotide exchange assays were performed to validate the in vitro activities of BI-2852 and BAY-293. The IC_{50} value of BI-2852 was 7.54 ± 1.35 μM, whereas BAY-293 showed better results, with an IC_{50} value of 85.08 ± 4.32 nM (Fig. 1b). Several KRAS variant recombinant proteins were purified to evaluate the selectivity of these two compounds. Nucleotide exchange assays were performed, and no obvious selectivity among KRAS variants were found, except KRAS G12C with a small selectivity window (approximately 5-fold) (Fig. 1c, Supplementary Table S1). These data suggest that BI-2852 and BAY-293 may serve as pan-KRAS inhibitors to block KRAS activation in vitro.

BI-2852 and BAY-293 inhibited proliferation of KRAS-driven cancer cells

To investigate the proliferative effects of pan-KRAS inhibitors in KRAS-driven cancer cells, a cell viability assay was performed. A

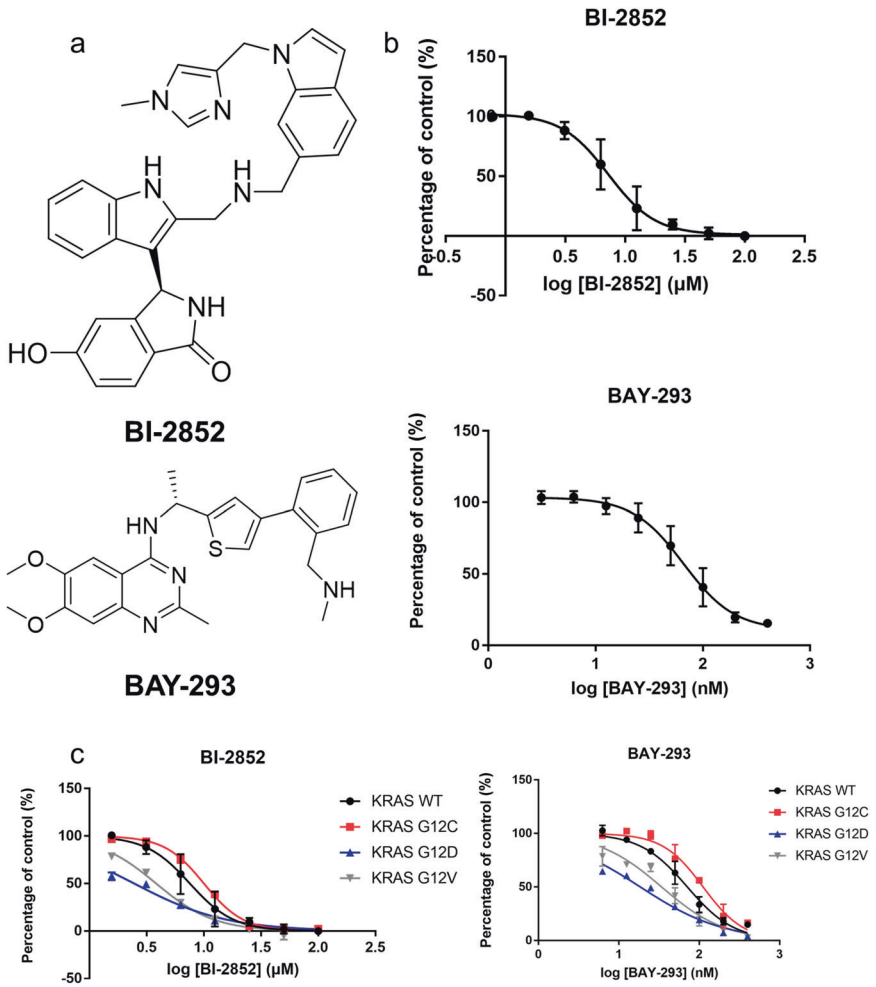

Fig. 1 BI-2852 and BAY-293 inhibited the activation of Kirsten rat sarcoma virus (KRAS) mediated by SOS1. a Chemical structures of BI-2852 (top) and BAY-293 (bottom). **b** Concentration-dependent inhibitory effects of BI-2852 (up) and BAY-293 (down) on the activation of $KRAS^{WT}$ mediated by SOS1, assessed using nucleotide exchange assay. Data are shown as mean ± SD from three independent experiments. **c** Concentration-dependent inhibition effects of BI-2852 (left) and BAY-293 (right) on the activation of KRAS variants mediated by SOS1, assessed by nucleotide exchange assay. Data are shown as mean ± SD from two or three independent experiments. The color key for the KRAS variant is shown.

CFSE cell proliferation assay was firm performed to determine the percentage of FBS used in cellular assays for cell culture and to monitor cell growth in 2D adherent monolayers. The results showed that BAY-293 significantly inhibited PDAC cell growth only at the highest concentration under normal serum conditions (Fig. 2a, b). Furthermore, compared to normal serum conditions, there was an increase in drug sensitivity when cells were cultured in low serum conditions. Therefore, 2% FBS was chosen as the culture condition for the subsequent cellular assay.

KRAS mutations drive tumorigenesis and development of many cancers. Three types of cancer were selected, namely NSCLC, CRC, and PDAC, to perform alamarBlue cell proliferation assays. Targeting KRAS G12C was proven to be an efficient therapeutic strategy for NSCLC, and AMG 510 was approved by the FDA in 2021 to treat NSCLC patients with the $KRAS^{G12C}$ mutation [22]. According to basic research on KRAS, differential drug sensitivity for targeting KRAS has been confirmed when examined under 2D adherent monolayer versus 3D spheroid culture conditions [32–34]. To assess the potency of pan-KRAS inhibitors in PDAC, NSCLC was used as the first disease model. The 12 different NSCLC cell lines were divided into two groups, *KRAS* WT and *KRAS* mutant groups, 3D cultured under low serum conditions, and treated with increasing concentrations of BI-2852 or BAY-293 for 6 d. BI-2852 and BAY-293 significantly reduced the growth of various NSCLC cell lines in a dose-dependent manner (Fig. 3a). The IC_{50} values of BI-2852 in NSCLC cell lines ranged from 4.63 to over 100 μM, whereas BAY-293 showed better efficiency with IC_{50} values ranging from 1.29 to 17.84 μM (Supplementary Table S2). There was no obvious difference in drug sensitivity between the *KRAS* WT and *KRAS* mutant groups for NSCLC.

CRC is a KRAS-driven cancer with poor prognosis [35]. To assess the potency of pan-KRAS inhibitors in PDAC, CRC was used as a second disease model, with 15 different CRC cell lines cultured and treated as described previously. The two pan-KRAS inhibitors inhibited the cell proliferation of multiple CRC cell lines; the IC_{50} values of BI-2852 ranged from 19.21 to over 100 μM, whereas IC_{50} values of BAY-293 ranged from 1.15 to 5.26 μM (Fig. 3b, Supplementary Table S3). There was no obvious difference in drug sensitivity between the *KRAS* WT and *KRAS* mutant groups for CRC.

In contrast to NSCLC and CRC, PDAC had a higher frequency of mutations. Therefore, only one *KRAS* WT PDAC cell line, BxPC-3, was used. Pan-KRAS inhibitors were profiled for their antiproliferative activity in five PDAC cell lines. BI-2852 showed weak growth inhibitory effect on PDAC cell lines, with IC_{50} values ranging from 18.83 to over 100 μM, whereas BAY-293 exhibited

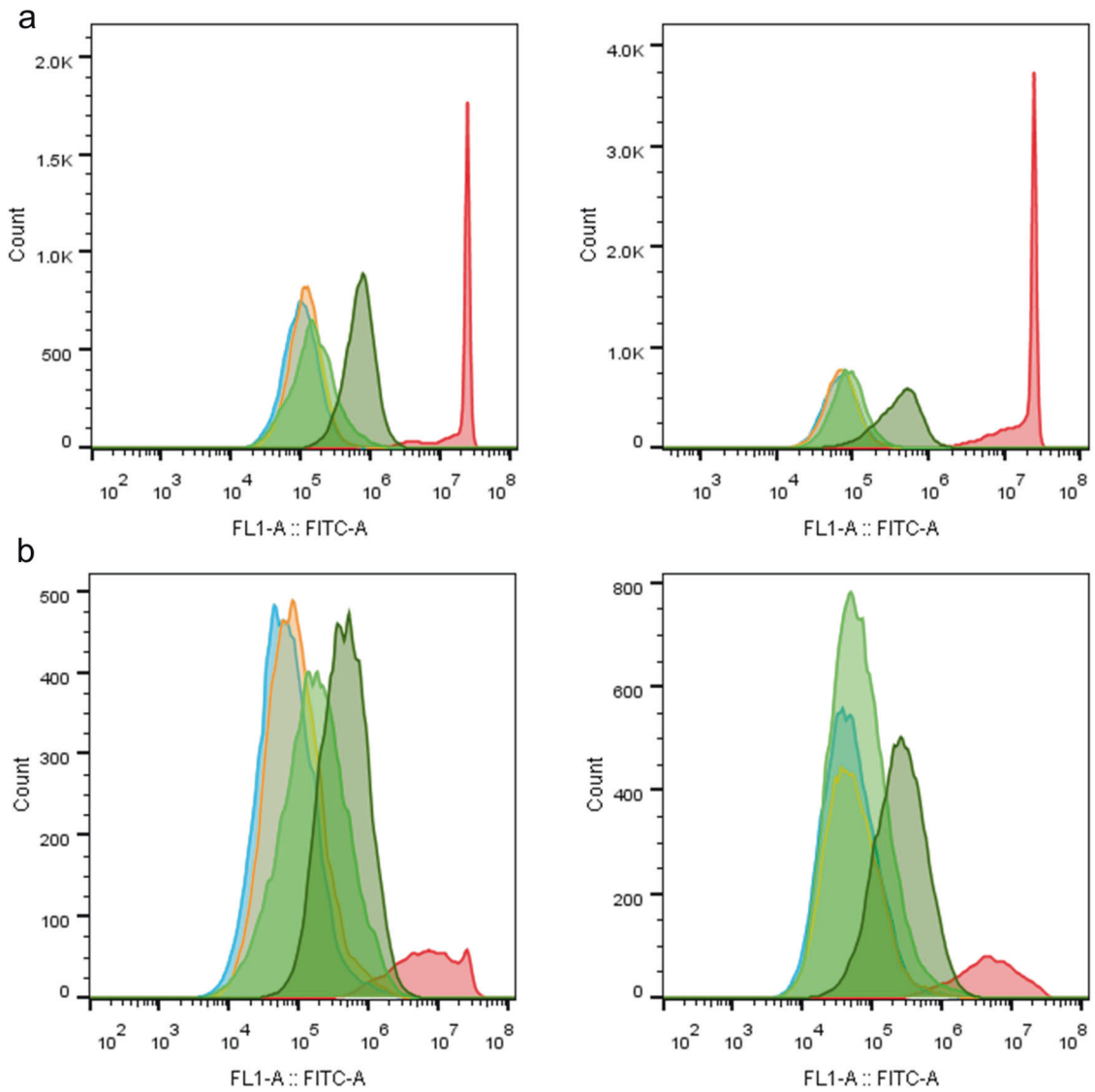

Fig. 2 BAY-293 slightly inhibited proliferation of Kirsten rat sarcoma virus (KRAS)-driven cancer cells in 2D culture. a MIA PaCa-2 cells were labeled with 5 μM and cultured in Dulbecco's Modified Eagle's Medium (DMEM) supplemented with 2% (left) or 10% fetal bovine serum (FBS) (right) and treated with dimethyl sulfoxide (DMSO) or BAY-293 for 4 day. The red peak represents cells analyzed immediately after labeling, the dark green peak represents cells treated with 5 μM BAY-293, the light green peak represents cells treated with 2.5 μM BAY-293, the orange peak represents cells treated with 1.25 μM BAY-293, and the blue peak represents cells treated with DMSO. **b** PANC-1 cells labeled with 5 μM were cultured in DMEM medium supplemented with 2% (left) or 10% FBS (right) and treated with DMSO or BAY-293 for 5 day. The red peak represents cells analyzed immediately after labeling, the dark green peak represents cells treated with 10 μM BAY-293, the light green peak represents cells treated with 5 μM BAY-293, the orange peak represents cells treated with 2.5 μM BAY-293, and the blue peak represents cells treated with DMSO.

complete growth suppression of KRAS mutant PDAC cell line, with IC_{50} values ranging from 0.95 to 6.64 μM and a small selectivity window in the KRAS alle (Fig. 3c, Supplementary Table S4). This result indicates that the pan-KRAS inhibitor BAY-293 may have a better therapeutic effect in PDAC than in NSCLC and CRC. In addition, approximately 90% of patients with PDAC carry at least one type of KRAS mutation allele, which makes pan-KRAS inhibitors more efficient in the treatment of PDAC. The BAY-293 showed lowest IC50 value in PDAC cell lines, with a small selectivity window between *KRAS* WT and mutant cell lines, and was effective in all PDAC cell lines.

Due to the limited potency of BI-2852, BAY-293 was chosen as a pharmacological probe to further study the therapeutic potential of pan-KRAS inhibitors in PDAC. These data indicated that BAY-293 inhibited cell growth in both 2D and 3D culture conditions but culturing in 3D conditions increased drug sensitivity, whereas low serum conditions may improve the antiproliferation effect.

BAY-293 regulated KRAS signaling pathway

The KRAS pathway is one of the most important signaling pathways controlling cell growth, proliferation, and survival in PDAC [8, 36–38]. To determine the effect of pan-KRAS inhibitors on PDAC, the PANC-1 (*p.G12D*) PDAC cell line was assessed following a 72-h treatment period with BAY-293. BAY-293 inhibited extracellular signal-regulated kinase (ERK) phosphorylation after 3 h of treatment. (Fig. 4a). A rebound of protein expression and phosphorylation levels in the KRAS signaling pathway was observed at 48 h (pERK) and 72 h (phosphorylated protein kinase B [pAKT]). Next, 24 h, the effective time point, was chosen as the treatment time for BAY-293 at gradient doses.

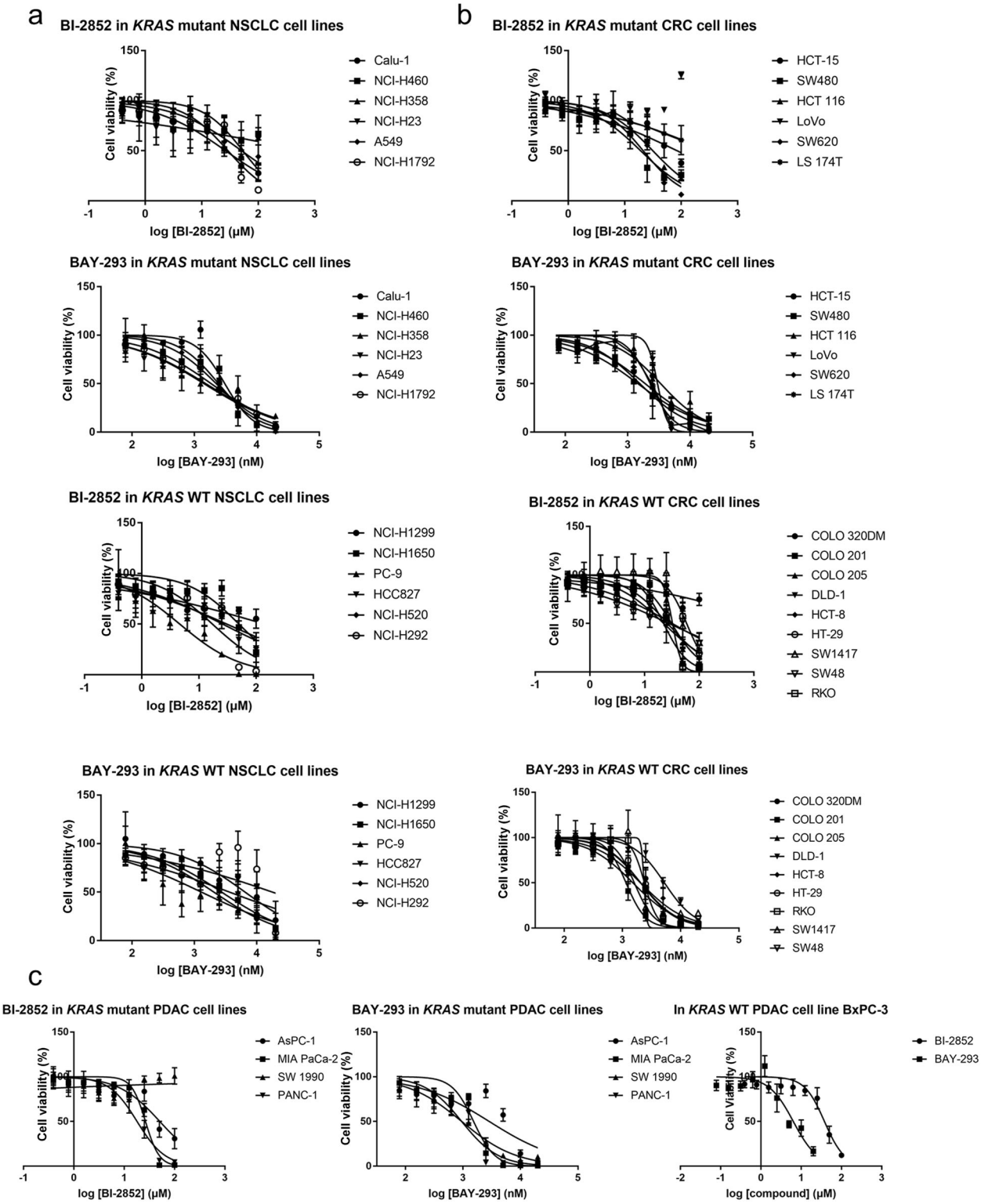

Consistent with the result of the 72 h treatment, BAY-293 reduced the phosphorylation of ERK, AKT, and S6 in a dose-dependent manner (Fig. 4b). However, a reverse trend was observed in another PDAC cell line, MIA PaCa-2 (*p.G12C*). BAY-293 promoted the phosphorylation of ERK and AKT in a dose-dependent manner in MIA PaCa-2 (Fig. 4c). We speculated that there were some feedback regulations determining cell fate, which was previously reported for SOS1 modulator compounds [39]. Interestingly, we observed an increased expression of cleaved poly (ADP-ribose) polymerase (PARP) (a marker of cell apoptosis) in MIA PaCa-2 cells treated with BAY-293. This implies that BAY-293 may inhibit PDAC proliferation through feedback regulation.

BAY-293 induced feedback regulation in PDAC

Based on the differences between PANC-1 and MIA PaCa-2 cells, RNA-seq analysis of the total RNA extracted from PANC-1 and MIA

Fig. 3 BI-2852 and BAY-293 inhibited proliferation of Kirsten rat sarcoma virus (KRAS)-driven cancer cells. a Dose response of the viability of various *KRAS* WT or *KRAS* mutant non-small cell lung cancer)NSCLC) cell lines exposed to BI-2852 and BAY-293 cultured in 3D spheroids and low serum conditions for 6 days, and cell viability was determined using alamarBlue. The cell viability of the drug-treated groups was normalized to that of the corresponding positive control dimethyl sulfoxide (DMSO)-treated groups. The points indicate the mean ± s.e.m of three independent experiments. The symbol key for the NSCLC cell lines is shown. **b** Dose response of the viability of various *KRAS* WT or *KRAS* mutant colorectal cancer (CRC) cell lines exposed to BI-2852 and BAY-293 cultured in 3D spheroids and low serum conditions for 6 days, and cell viability was determined using alamarBlue. The cell viability of the drug-treated groups was normalized to that of the corresponding positive control DMSO-treated groups. The points indicate the mean ± s.e.m. of three independent experiments. The symbol key for the CRC cell lines is shown. **c** Dose response of the viability of various *KRAS* WT or *KRAS* mutant pancreatic ductal adenocarcinoma (PDAC) cell lines exposed to BI-2852 and BAY-293 cultured in 3D spheroids and low serum conditions for 6 days, and cell viability was determined using alamarBlue. The cell viability of the drug-treated groups was normalized to that of the corresponding positive control DMSO-treated groups. The points indicate the mean ± s.e.m. of three independent experiments. The symbol key for the PDAC cell lines is shown.

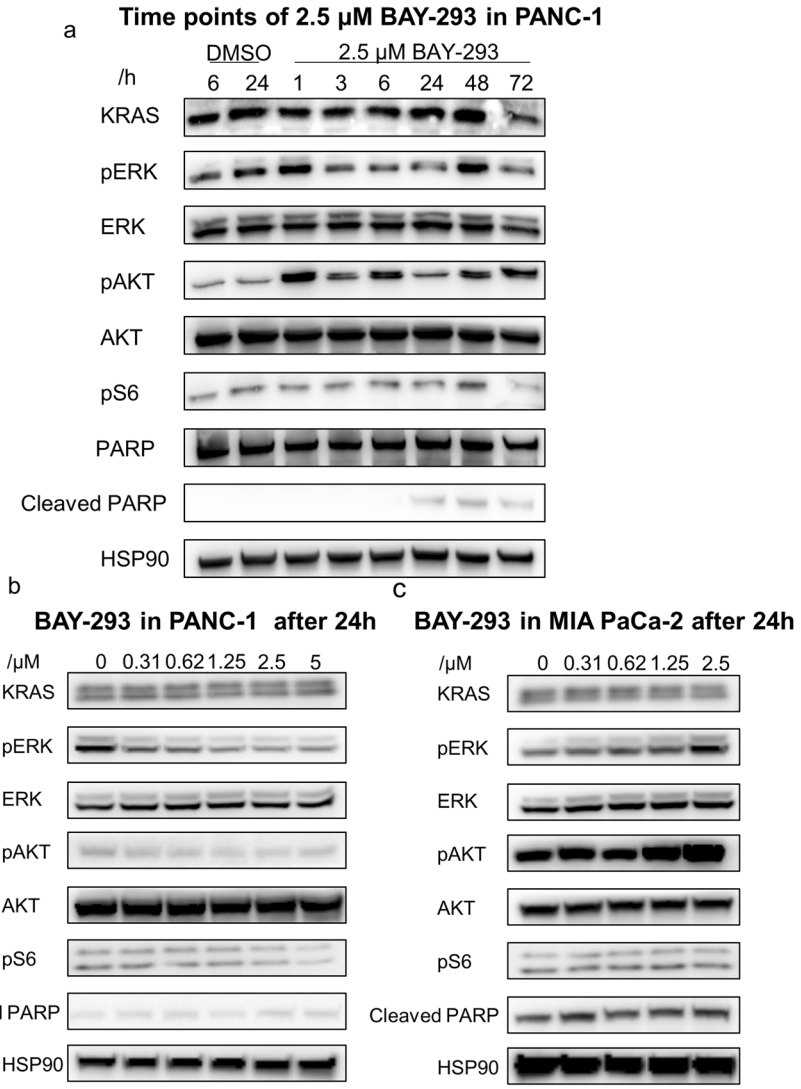

Fig. 4 BAY-293 regulated Kirsten rat sarcoma virus (KRAS) signaling pathway. a Western blot analysis of KRAS signaling pathway targets in PANC-1 cells treated from 1 h to 72 h with BAY-293 at 2.5 μmol/L. HSP90 was used as a loading control. **b** Western blot analyses of KRAS signaling pathway targets in PANC-1 cells treated for 24 h with BAY-293 over a 5-point dose response. HSP90 was used as a loading control. **c** Western blot analyses of KRAS signaling pathway targets in MIA PaCa-2 cells treated for 24 h with BAY-293 over a 4-point dose response. HSP90 was used as a loading control.

PaCa-2 cells treated with DMSO or BAY-293 was performed to explore the pharmacological mechanism of pan-KRAS inhibitors. To address this, we compared the differentially expressed genes (DEGs) between the two cell lines. There were 51 genes that varied in both PDAC cell lines, with 111 genes expressed differently in PANC-1 alone, whereas 1364 differential genes were only observed in MIA PaCa-2, in which components of the KRAS showed unexpectedly increased phosphorylation levels (Fig. 5a). The top differentially expressed genes are marked in Fig. 5b, including which included *PER1, CDKN1C, GADD45B, DUSP2, TXNIP, ZFP36, DRD4, BBC3, RIN1, FGFR3, RGS14, MKI67*, and *PPP1R10* related to KRAS signaling and apoptosis. Meanwhile, the top 40 significantly differentially expressed genes were clustered and are displayed in Fig. 5c, related to several cellular processes,

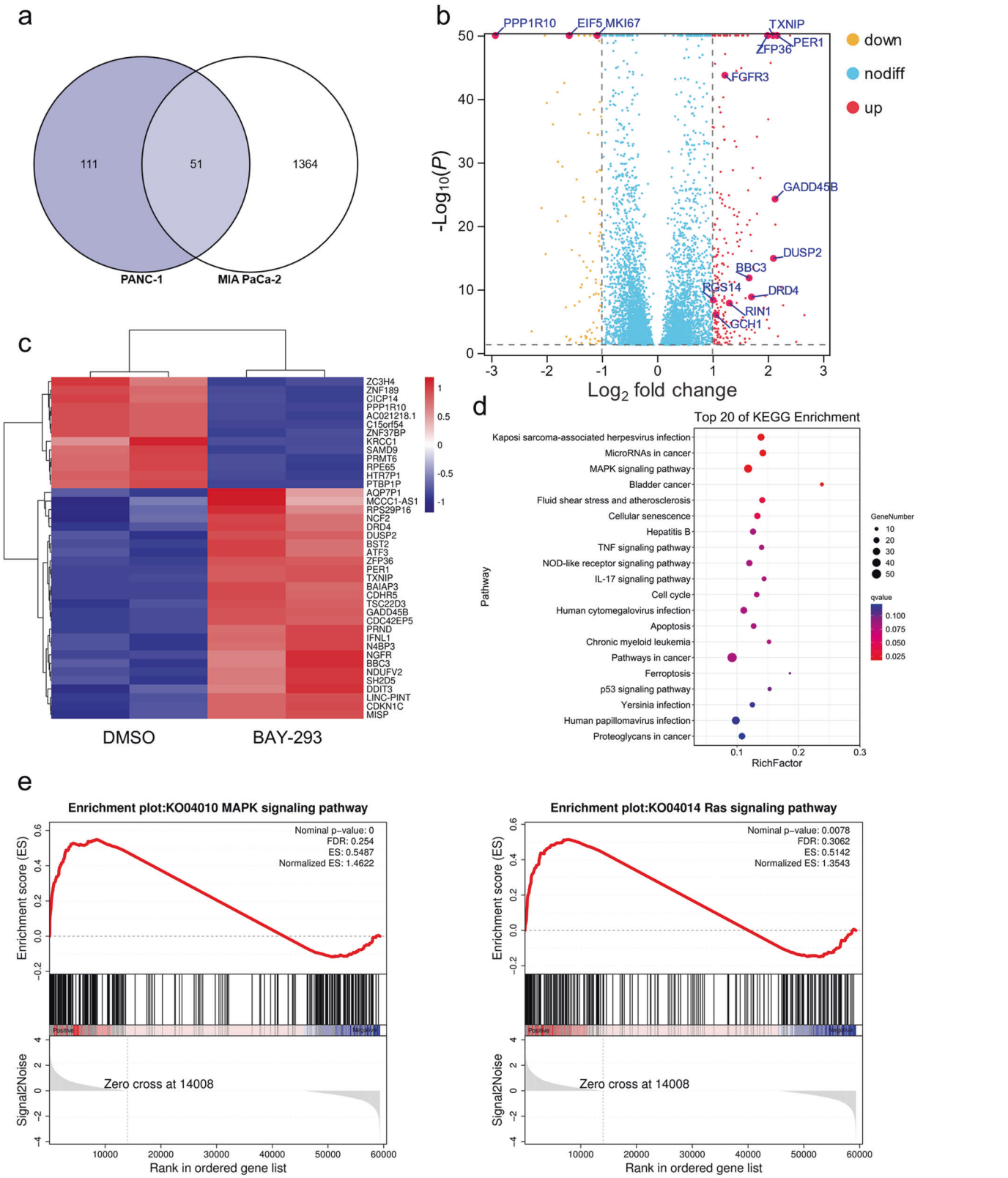

Fig. 5 BAY-293 induced feedback regulations in pancreatic ductal adenocarcinoma (PDAC). a Venn diagram illustrating the overlap of differentially expressed genes (DEGs) between PANC-1 cells treated with 5 μM BAY-293 versus dimethyl sulfoxide (DMSO) and MIA PaCa-2 cells treated with 2.5 μM BAY-293 versus DMSO with FDR < 0.05. **b** Volcano plots displaying differentially expressed genes in MIA PaCa-2 cells 48 h after treatment with DMSO or 2.5 μM BAY-293. Significance is denoted in the legend (FDR < 0.01). **c** Hierarchical clustering of the top 40 differentially regulated genes (FDR < 0.05) following treatment with BAY-293 (2.5 μM) or DMSO for 48 h. Two independent biological replicates per group. **d** The Kyoto Encyclopedia of Genes and Genomes (KEGG) pathway enrichment analysis performed on MIA PaCa-2 cells treated with BAY-293 (2.5 μM). Top 20 KEGG enrichment pathways. **e** GSEA plots showing representative gene set enrichment analyses (nominal $P < 0.01$) following BAY-293 treatment.

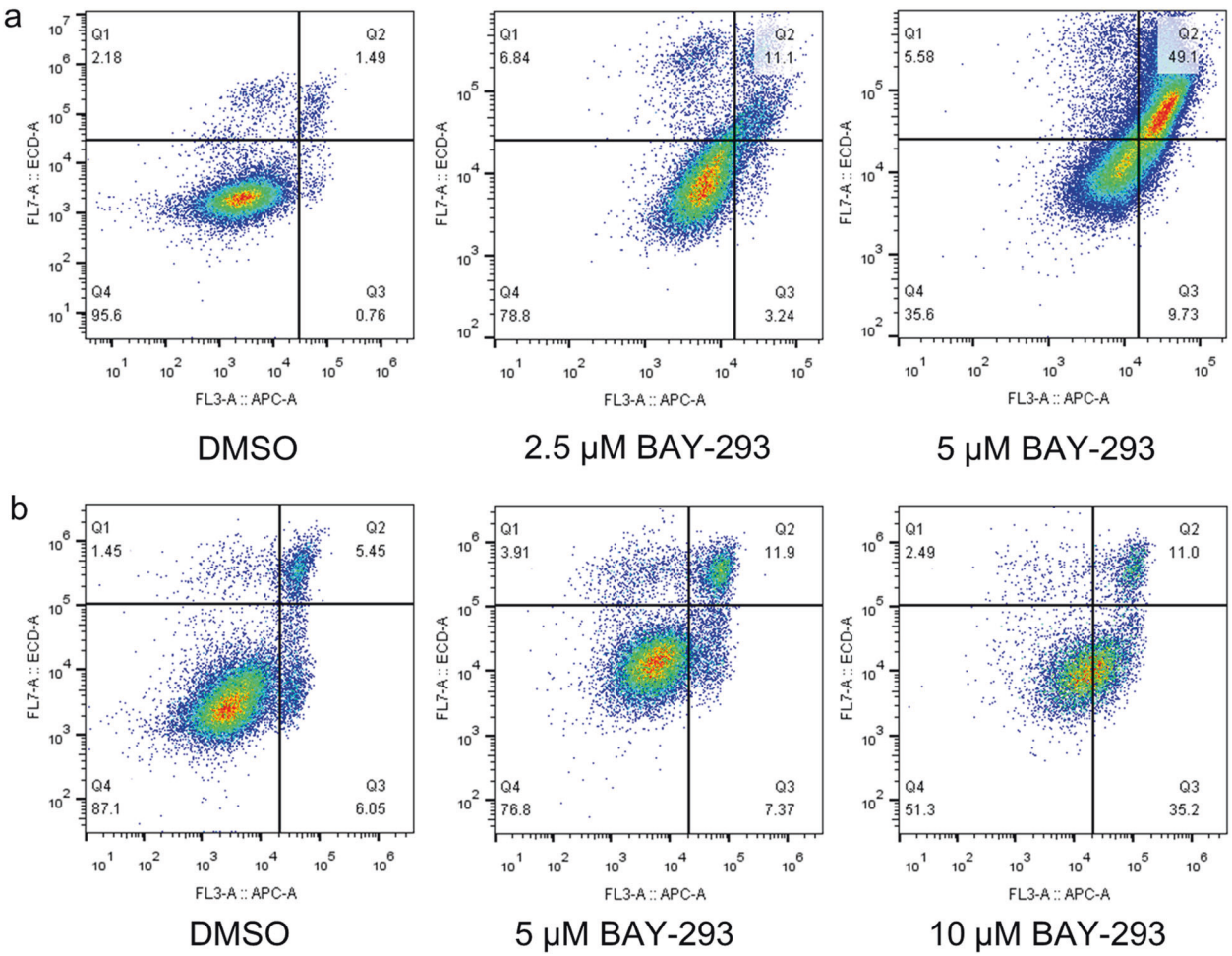

Fig. 6 BAY-293 promoted pancreatic ductal adenocarcinoma (PDAC) cell apoptosis. a MIA PaCa-2 cells were cultured in 2% fetal bovine serum (FBS) and exposed to BAY-293 (0, 2.5, and 5 μM) for 48 h, and Annexin V-APC/propidium iodide (PI) staining analysis was conducted to evaluate the percentage of apoptotic cells using flow cytometry. **b** PANC-1 cells were cultured in 2% FBS and exposed to BAY-293 (0, 5, and 10 μM) for 48 h, and Annexin V-APC/PI staining analysis was conducted to evaluate the percentage of apoptotic cells using flow cytometry.

including cell growth and apoptosis. Enrichment analysis of the Kyoto Encyclopedia of Genes and Genomes (KEGG) pathway showed that BAY-293 broadly affected multiple pathways, such as the mitogen activated protein kinase (MAPK) signaling pathway and apoptosis, which provided further insight into the molecular mechanism pertinent to its antitumor activity (Fig. 5d). Gene ontology (GO) enrichment analysis suggested that BAY-293 regulates numerous molecular functions linked to Ras GTP binding, GTPase activity, and MAP kinase tyrosine/serine/threonine phosphatase activity (Supplementary Fig. S1). To further investigate the regulatory effect of BAY-293 on Ras-related genes and pathways, gene set enrichment analysis (GSEA)was performed and it was found that BAY-293 significantly induced the expression of MAPK signaling and Ras signaling pathway gene sets in MIA PaCa-2, which proved feedback regulation in this PDAC cell line (Fig. 5e). Collectively, these gene expression analyses revealed the regulatory effect of BAY-293 in PDAC, further supporting the notion that BAY-293 functions via complex feedback regulation.

BAY-293 promoted PDAC cell apoptosis

Immunoblotting and RNA-seq results revealed that pan-KRAS inhibitors may inhibit cell proliferation by promoting apoptosis. Therefore, flow cytometry was used to monitor apoptosis after BAY-293 treatment. Based on the immunoblotting results for PANC-1, cleaved PARP showed the highest expression level after 48 h of treatment. PDAC cells were exposed to BAY-293 for 48 h, followed by an Annexin V/PI double staining assay using flow cytometry. The results showed that treatment with BAY-293 for 48 h significantly promoted apoptosis in MIA PaCa-2 cells but not in PANC-1 cells (Figs. 6a, b).

BAY-293 inhibited cell growth of PDAC patient-derived organoids

BAY-293 showed broad and robust antiproliferation effects in PDAC in the cell-based assays of this study, but its poor bioavailability limits its usage in vivo [25, 40]. Recently, organoids have been considered as physiologically relevant in vitro models for cancer research and drug screening, with high establishing efficiency and patient-personalized genetic characteristics [41]. Therefore, PDOs were chosen as the disease model to mirror responses in vivo to evaluate the antitumor activity in PDAC of BAY-293. Eleven primary tumor samples were obtained from pancreatic tumor surgical resections to establish PDAC organoid cultures, and 10 organoids of which 11 samples were established. The first PDAC0 sample that failed to generate an organoid culture was digested for a long time, resulting in insufficient living cells for organoid formation. Organoid culture PDAC1 (derived from Shanghai General Hospital pancreatic ductal adenocarcinoma patient #1) was imaged every 2 d, which showed dynamic organoid behaviors with cell growth and death (Fig. 7a). Simultaneously, we captured pictures of the wilder view with a 4× objective of the PDO culture every day and monitored cell

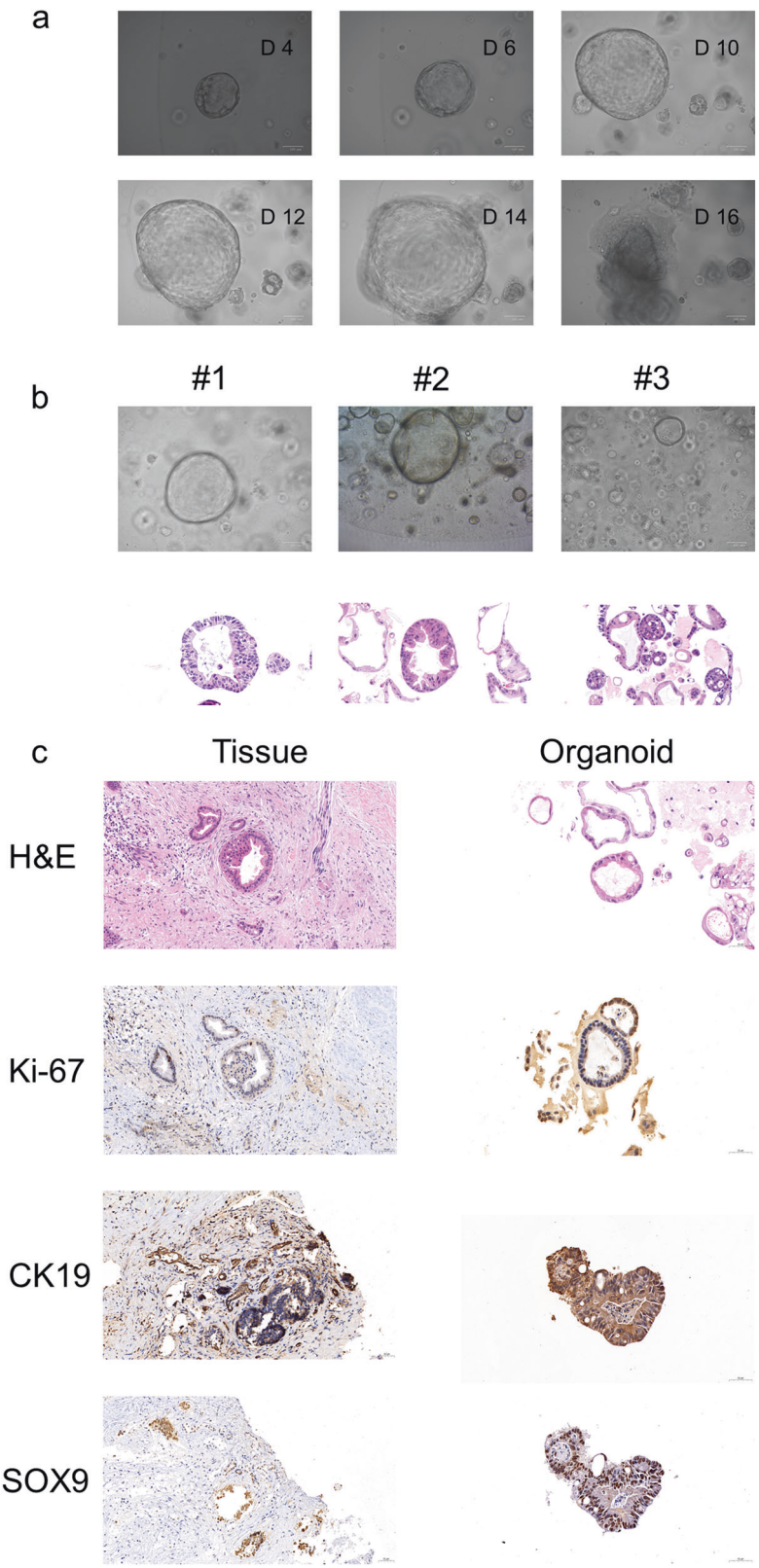

Fig. 7 Modeling human pancreatic ductal adenocarcinoma (PDAC) with patient-derived organoids. a Time-lapse imaging sequence of the PADC#1 organoids. Representative images (20× objective magnification) are shown. Scale bars, 100 μm. **b** Microscopy and hematoxylin and eosin (H&E) staining images of PDAC #1, #2, and #3. Representative images (microscopy image, ×10 magnification; H&E staining images, 40× objective magnification) are shown. Scale bars, 100 μm. **c** H&E and immunohistochemistry images of Ki-67, CK19, and SOX9 staining in tumor organoids and matched primary tumors. Representative images (Tissue, 20× objective magnification; Organoids, 30× objective magnification) are shown. Scale bars, 50 μm.

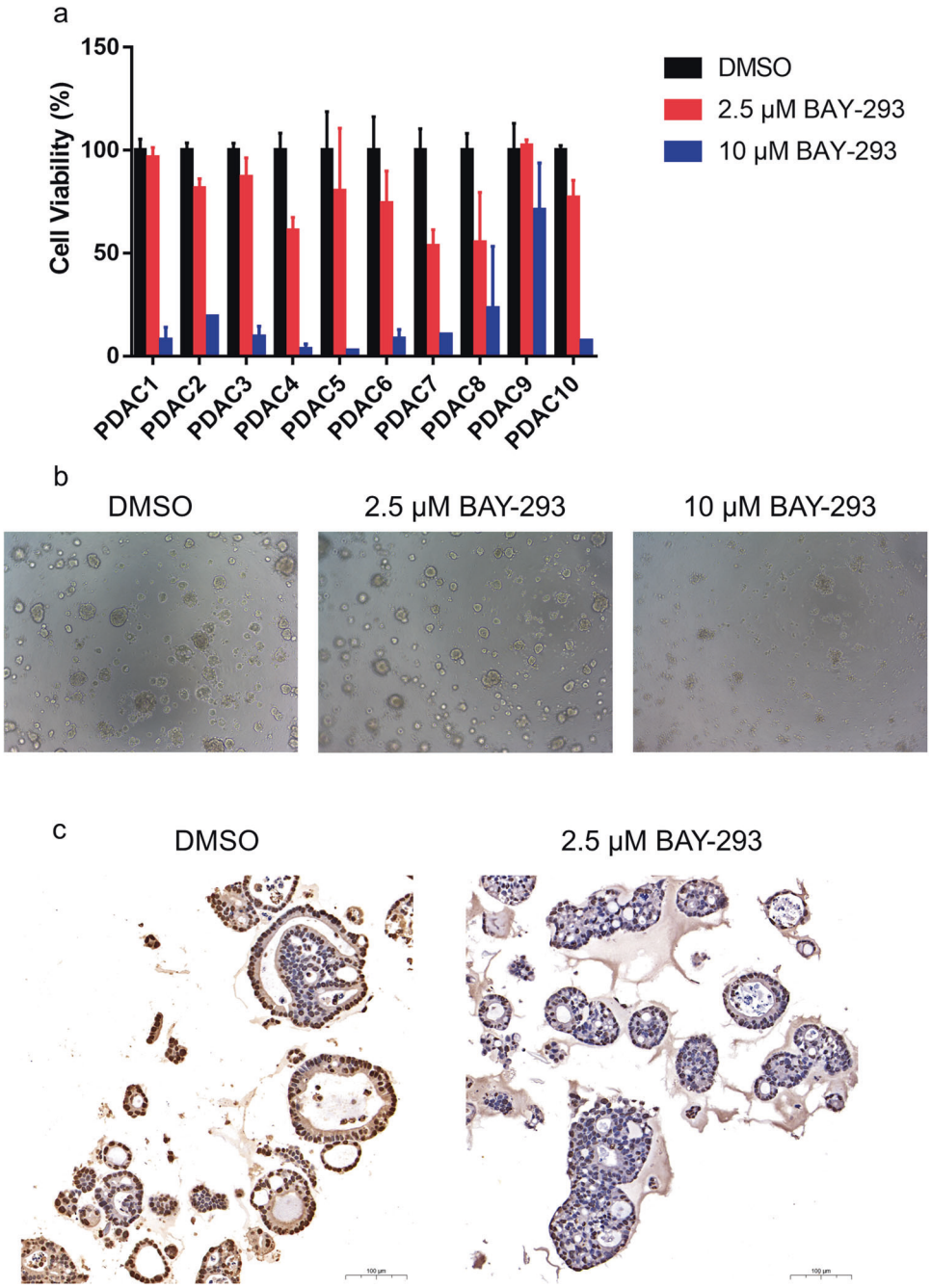

Fig. 8 BAY-293 inhibited cell growth of pancreatic ductal adenocarcinoma (PDAC) patient-derived organoids. a Cell viability assay results of PDAC organoid cultures treated with dimethyl sulfoxide (DMSO), 2.5 μM BAY-293, or 10 μM BAY-293 for 6 days. The results were normalized to those of DMSO-treated organoids. The color key for drug concentration is shown. **b** Representative images (10× objective magnification) of PDAC organoid cultures treated with DMSO, 2.5 μM BAY-293, or 10 μM BAY-293 for 6 days. **c** Immunohistochemistry image (15× objective magnification) of Ki-67 staining in PDAC organoid cultures treated with DMSO or 2.5 μM BAY-293. Scale bars, 100 μm.

growth using a cell viability assay (Supplementary Fig. S2a). Next, we analyzed the histoarchitecture of tumor organoids after 12 days of culture, and all three organoids showed clear and similar morphological structures on hematoxylin-eosin (H&E) staining (Fig. 7b). We next analyzed the histoarchitecture, biomarkers, and proliferation status of both patient tissue and PDO culture, which showed high similarities in morphological structure and tumor progression (Fig. 7c). Thus, these results revealed that our PDOs conserved the histological organization and tumor progression characteristics observed in PDAC patients' primary tissue and might serve as an ideal in vitro disease model for drug sensitivity testing of compounds with limited bioavailability.

PDOs derived from ten independent patient tumors (PDAC1 to PDAC10) were further analyzed. All cultures were treated with DMSO or BAY-293 for 6 d. BAY-293 treatment effectively inhibited the proliferation of PDOs at a dose of 10 μM, indicating potential in vivo antitumor activity, although there were significant drug sensitivity differences among PDOs (Fig. 8a). According to the *KRAS* genotype identification of patient samples, PDO with $KRAS^{G13D}$ genotype might have lower sensitivity towards pan-KRAS inhibitor BAY-293, consistent with the cell viability results in

cancer cell lines (Fig. 3a, b, and Supplementary Tables S5, S6). The antiproliferation results could also be directly observed using microscopy (Fig. 8b). IHC staining showed that PDO regression was associated with reduced Ki67 levels in PDOs after BAY-293 treatment (Fig. 8c). Together, these data indicate the therapeutic potential of BAY-293 for PDAC treatment.

DISCUSSION

PDAC is the deadliest cancer type worldwide without an effective therapeutic strategy [4]. *KRAS* is the most frequently mutated gene in PDAC, with gain-of-function alterations driving tumorigenesis and development [42]. Therefore, targeting KRAS is a promising therapeutic strategy for PADC [43–50]. However, due to universal tumor heterogeneity in PDAC, pan-KRAS inhibitors may serve as an optimum solution [21]. Thus, there is generally more than one KRAS mutant genotype in PDAC tumors. Two pan-KRAS inhibitors were reported in 2019, BI-2852 [24] and BAY-293 [25], and they were used as pharmacological probes to investigate the application benefit of targeting KRAS and the therapeutic effect of pan-KRAS inhibitors in PDAC.

This work demonstrated that BI-2852 and BAY-293 inhibited KRAS activation by SOS1 in vitro, with slight selectivity among oncogenic KRAS mutants. Meanwhile, BAY-293 limited the growth of PDAC cell lines, showing effective antiproliferative activity with sub-micromolar IC_{50} values in 3D spheroid culture conditions with a small selectivity window. Interestingly, feedback regulation in PDAC weakened the antitumor activity of BAY-293, resulting in a 50 times differences from the i*n vitro* study, which was confirmed using immunoblotting and RNA-seq analyses. PDAC PDOs were used as a disease model and the therapeutic potential of BAY-293 in PADC treatment was profiled. Collectively, pan-KRAS inhibitors showed effective antitumor activity in PDAC; however, the emergence of feedback regulation impaired drug sensitivity.

Consistent with previous results [33, 51], differences between 2D monolayer and 3D spheroid cultures were revealed. Pan-KRAS inhibitors were more effective under 3D culture conditions. Low serum conditions that reduce GTP concentration in the cytoplasm and cause a decrease in GTP-loaded KRAS may increase the drug sensitivity of PDAC cells to pan-KRAS inhibitors, which block the activation of KRAS. In addition, feedback regulation plays an important role in the molecular mechanisms of action of pan-KRAS inhibitors. According to the reported KRAS regulators, feedback regulation can reverse the activation effect of SOS1 and KRAS activators, resulting in the inhibition of cell growth in cancer cells [52, 53]. Our immunoblotting and RNA-Seq analyses provide evidence of feedback regulation and direction of investigation. Furthermore, it was found that apoptosis mediated the antitumor activity in MIA PaCa-2, whereas it was not clear in PANC-1 even though the IC_{50} values of these two cell lines were similar. Based on the RNA-Seq analysis, lysosomes, ferroptosis, and autophagy may be involved in cell fate determination in PANC-1; however, the exact antiproliferation mechanism and molecular interaction remain unclear.

Recently, more pan-KRAS inhibitors have been reported [54–56] and allosteric regulation provides another direction for drugging KRAS [57–63]. BI-3406 is the front page of drug discovery research, with higher efficiency and selectivity than BAY-293. Based on the antitumor activity of BAY-293 in PDAC, BI-3406 is a promising pan-KRAS inhibitor that may be used as a future clinical therapeutic strategy for patients with PDAC.

Collectively, this study demonstrated that the two pan-KRAS inhibitors, BI-2852 and BAY-293, robustly inhibited the interaction between KRAS and SOS1, showing effective in vitro antitumor potency in PDAC, with feedback regulation involved in the mechanism of drug action. The drug development potential of pan-KRAS inhibitors for PDAC was verified in this work. These results provide a sufficient theoretical basis for KRAS as a clinical therapeutic target and for the application of KRAS inhibitors in the treatment of PDAC, which has important scientific significance in translational medicine.

ACKNOWLEDGEMENTS

This work was partly supported by grants from the National Natural Science Foundation of China (81925034, 22077082, 91753117, and 81721004), Innovation Program of Shanghai Municipal Education Commission (2019-01-07-00-01-E00036, China), Shanghai Science and Technology Innovation (19431901600, China), Shanghai Health and Family Planning System Excellent Subject Leader and Excellent Young Medical Talents Training Program (2018BR12, China), CAMS Innovation Fund for Medical Sciences (CIFMS) (2019-I2M-5-051), and Shanghai Frontiers Science Center of Cellular Homeostasis and Human Diseases.

AUTHOR CONTRIBUTIONS

SYL and JZ conceived and designed the experiments; CXW and TTW performed the experiments and analyzed the data; KDZ provided patient samples for PDO culture; MYL and QCS visualized the data; SYL and JZ contributed reagents, materials, and analytical tools. CXW wrote the original manuscript and SYL edited and revised the manuscript. All authors have read and agreed to the published version of the manuscript.

ADDITIONAL INFORMATION

Supplementary information The online version contains supplementary material available at https://doi.org/10.1038/s41401-022-00897-4.

Competing interests: The authors declare no competing interests.

REFERENCES

1. Ekbom A, McLaughlin JK, Karlsson B-M, Nyrén O, Gridley G, Adami H-O, et al. Pancreatitis and pancreatic cancer: a population-based study. JNCI: J Natl Cancer Inst. 1994;86:625–7.
2. Kleeff J, Korc M, Apte M, La Vecchia C, Johnson CD, Biankin AV, et al. Pancreatic cancer. Nat Rev Dis Prim. 2016;2:16022.
3. Siegel RL, Miller KD, Fuchs HE, Jemal A. Cancer statistics, 2021. CA Cancer J Clin. 2021;71:7–33.
4. Neoptolemos JP, Kleeff J, Michl P, Costello E, Greenhalf W, Palmer DH. Therapeutic developments in pancreatic cancer: current and future perspectives. Nat Rev Gastroenterol Hepatol. 2018;15:333–48.
5. Conroy T, Hammel P, Hebbar M, Ben Abdelghani M, Wei AC, Raoul JL, et al. FOLFIRINOX or gemcitabine as adjuvant therapy for pancreatic cancer. N Engl J Med. 2018;379:2395–406.
6. Binenbaum Y, Na'ara S, Gil Z. Gemcitabine resistance in pancreatic ductal adenocarcinoma. Drug Resist Updat. 2015;23:55–68.
7. Zheng C, Jiao X, Jiang Y, Sun S. ERK1/2 activity contributes to gemcitabine resistance in pancreatic cancer cells. J Int Med Res. 2013;41:300–6.
8. Jones S, Zhang X, Parsons DW, Lin JC, Leary RJ, Angenendt P, et al. Core signaling pathways in human pancreatic cancers revealed by global genomic analyses. Science. 2008;321:1801–6.
9. Lohr M, Kloppel G, Maisonneuve P, Lowenfels AB, Luttges J. Frequency of K-ras mutations in pancreatic intraductal neoplasias associated with pancreatic ductal adenocarcinoma and chronic pancreatitis: a meta-analysis. Neoplasia. 2005;7:17–23.
10. Iodice S, Gandini S, Maisonneuve P, Lowenfels AB. Tobacco and the risk of pancreatic cancer: a review and meta-analysis. Langenbecks Arch Surg. 2008;393:535–45.
11. Buscail L, Bournet B, Cordelier P. Role of oncogenic KRAS in the diagnosis, prognosis and treatment of pancreatic cancer. Nat Rev Gastroenterol Hepatol. 2020;17:153–68.
12. Pylayeva-Gupta Y, Lee KE, Hajdu CH, Miller G, Bar-Sagi D. Oncogenic Kras-induced GM-CSF production promotes the development of pancreatic neoplasia. Cancer Cell. 2012;21:836–47.
13. Lu S, Jang H, Muratcioglu S, Gursoy A, Keskin O, Nussinov R, et al. Ras conformational ensembles, allostery, and signaling. Chem Rev. 2016;116:6607–65.
14. Lu S, Jang H, Gu S, Zhang J, Nussinov R. Drugging Ras GTPase: a comprehensive mechanistic and signaling structural view. Chem Soc Rev. 2016;45:4929–52.
15. Simanshu DK, Nissley DV, McCormick F. RAS proteins and their regulators in human disease. Cell. 2017;170:17–33.
16. Vetter IR, Wittinghofer A. The guanine nucleotide-binding switch in three dimensions. Science. 2001;294:1299–304.

17. Bos JL, Rehmann H, Wittinghofer A. GEFs and GAPs: critical elements in the control of small G proteins. Cell. 2007;129:865–77.
18. Miller MS, Miller LD. RAS mutations and oncogenesis: not all RAS mutations are created equally. Front Genet. 2011;2:100.
19. Jonckheere N, Vasseur R, Van, Seuningen I. The cornerstone K-RAS mutation in pancreatic adenocarcinoma: From cell signaling network, target genes, biological processes to therapeutic targeting. Crit Rev Oncol Hematol. 2017;111:7–19.
20. Moore AR, Rosenberg SC, McCormick F, Malek S. RAS-targeted therapies: is the undruggable drugged? Nat Rev Drug Discov. 2020;19:533–52.
21. Bannoura SF, Uddin MH, Nagasaka M, Fazili F, Al-Hallak MN, Philip PA, et al. Targeting KRAS in pancreatic cancer: new drugs on the horizon. Cancer Metastasis Rev. 2021;40:819–35.
22. FDA Approves First KRAS Inhibitor: Sotorasib. Cancer Discov. 2021;11:OF4-OF.
23. Peng J, Sun BF, Chen CY, Zhou JY, Chen YS, Chen H, et al. Single-cell RNA-seq highlights intra-tumoral heterogeneity and malignant progression in pancreatic ductal adenocarcinoma. Cell Res. 2019;29:725–38.
24. Kessler D, Gmachl M, Mantoulidis A, Martin LJ, Zoephel A, Mayer M, et al. Drugging an undruggable pocket on KRAS. Proc Natl Acad Sci USA. 2019;116:15823–9.
25. Hillig RC, Sautier B, Schroeder J, Moosmayer D, Hilpmann A, Stegmann CM, et al. Discovery of potent SOS1 inhibitors that block RAS activation via disruption of the RAS-SOS1 interaction. Proc Natl Acad Sci USA. 2019;116:2551–60.
26. Abraham SJ, Muhamed I, Nolet R, Yeung F, Gaponenko V. Expression, purification, and characterization of soluble K-Ras4B for structural analysis. Protein Expr Purif. 2010;73:125–31.
27. Maurer T, Garrenton LS, Oh A, Pitts K, Anderson DJ, Skelton NJ, et al. Small-molecule ligands bind to a distinct pocket in Ras and inhibit SOS-mediated nucleotide exchange activity. Proc Natl Acad Sci USA. 2012;109:5299–304.
28. van de Wetering M, Francies HE, Francis JM, Bounova G, Iorio F, Pronk A, et al. Prospective derivation of a living organoid biobank of colorectal cancer patients. Cell. 2015;161:933–45.
29. Boj SF, Hwang CI, Baker LA, Chio II, Engle DD, Corbo V, et al. Organoid models of human and mouse ductal pancreatic cancer. Cell. 2015;160:324–38.
30. Sun Q, Burke JP, Phan J, Burns MC, Olejniczak ET, Waterson AG, et al. Discovery of small molecules that bind to K-Ras and inhibit Sos-mediated activation. Angew Chem Int Ed. 2012;51:6140–3.
31. Jeng HH, Taylor LJ, Bar-Sagi D. Sos-mediated cross-activation of wild-type Ras by oncogenic Ras is essential for tumorigenesis. Nat Commun. 2012;3:1168.
32. Patricelli MP, Janes MR, Li LS, Hansen R, Peters U, Kessler LV, et al. Selective inhibition of oncogenic KRAS output with small molecules targeting the inactive state. Cancer Discov. 2016;6:316–29.
33. Janes MR, Zhang J, Li LS, Hansen R, Peters U, Guo X, et al. Targeting KRAS mutant cancers with a covalent G12C-specific inhibitor. Cell. 2018;172:578–89.
34. Fujita-Sato S, Galeas J, Truitt M, Pitt C, Urisman A, Bandyopadhyay S, et al. Enhanced MET translation and signaling sustains K-Ras–Driven proliferation under anchorage-independent growth conditions. Cancer Res. 2015;75:2851–62.
35. Porru M, Pompili L, Caruso C, Biroccio A, Leonetti C. Targeting KRAS in metastatic colorectal cancer: current strategies and emerging opportunities. J Exp Clin Cancer Res. 2018;37:57.
36. Matsuo Y, Campbell PM, Brekken RA, Sung B, Ouellette MM, Fleming JB, et al. K-Ras promotes angiogenesis mediated by immortalized human pancreatic epithelial cells through mitogen-activated protein kinase signaling pathways. Mol Cancer Res. 2009;7:799–808.
37. Zhang W, Nandakumar N, Shi Y, Manzano M, Smith A, Graham G, et al. Downstream of mutant KRAS, the transcription regulator YAP is essential for neoplastic progression to pancreatic ductal adenocarcinoma. Sci Signal. 2014;7:ra42.
38. Bailey P, Chang DK, Nones K, Johns AL, Patch AM, Gingras MC, et al. Genomic analyses identify molecular subtypes of pancreatic cancer. Nature. 2016;531:47–52.
39. Howes JE, Akan DT, Burns MC, Rossanese OW, Waterson AG, Fesik SW. Small molecule-mediated activation of RAS elicits biphasic modulation of phospho-ERK levels that are regulated through negative feedback on SOS1. Mol Cancer Ther. 2018;17:1051–60.
40. Theard PL, Sheffels E, Sealover NE, Linke AJ, Pratico DJ, Kortum RL. Marked synergy by vertical inhibition of EGFR signaling in NSCLC spheroids shows SOS1 is a therapeutic target in EGFR-mutated cancer. Elife. 2020;9:e58204.
41. Drost J, Clevers H. Organoids in cancer research. Nat Rev Cancer. 2018;18:407–18.
42. Bournet B, Buscail C, Muscari F, Cordelier P, Buscail L. Targeting KRAS for diagnosis, prognosis, and treatment of pancreatic cancer: Hopes and realities. Eur J Cancer. 2016;54:75–83.
43. Pantsar T. The current understanding of KRAS protein structure and function. Comput Struct Biotechnol J. 2020;18:189–98.
44. Vatansever S, Erman B, Gümüş ZH. Comparative effect of oncogenic mutations G12C, G12V, G13D, and Q61H on local conformations and dynamics of K-Ras. Comput Struct Biotechnol J. 2020;18:1000–11.
45. Lu S, Ni D, Wang C, He X, Lin H, Wang Z, et al. Deactivation pathway of Ras GTPase underlies conformational substates as targets for drug design. Acs Catal. 2019;9:7188–96.
46. Ni D, Li X, He X, Zhang H, Zhang J, Lu S. Drugging K-RasG12C through covalent inhibitors: mission possible? Pharmacol Ther. 2019;202:1–17.
47. Qiu Y, Wang Y, Chai Z, Ni D, Li X, Pu J, et al. Targeting RAS phosphorylation in cancer therapy: Mechanisms and modulators. Acta Pharm Sin B. 2021;11:3433–46.
48. Wang Y, Ji D, Lei C, Chen Y, Qiu Y, Li X, et al. Mechanistic insights into the effect of phosphorylation on Ras conformational dynamics and its interactions with cell signaling proteins. Comput Struct Biotechnol J. 2021;19:1184–99.
49. Jang H, Zhang M, Nussinov R. The quaternary assembly of KRas4B with Raf-1 at the membrane. Comput Struct Biotechnol J. 2020;18:737–48.
50. Tripathi S, Dsouza NR, Mathison AJ, Leverence E, Urrutia R, Zimmermann MT. Enhanced interpretation of 935 hotspot and non-hotspot RAS variants using evidence-based structural bioinformatics. Comput Struct Biotechnol J. 2021;20:117–27.
51. Hallin J, Engstrom LD, Hargis L, Calinisan A, Aranda R, Briere DM, et al. The KRAS (G12C) inhibitor MRTX849 provides insight toward therapeutic susceptibility of KRAS-mutant cancers in mouse models and patients. Cancer Discov. 2020;10:54–71.
52. Sarkar D, Olejniczak ET, Phan J, Coker JA, Sai J, Arnold A, et al. Discovery of sulfonamide-derived agonists of SOS1-mediated nucleotide exchange on RAS using fragment-based methods. J Med Chem. 2020;63:8325–37.
53. Xu K, Park D, Magis AT, Zhang J, Zhou W, Sica GL, et al. Small molecule KRAS agonist for mutant KRAS cancer therapy. Mol Cancer. 2019;18:85.
54. Hofmann MH, Gmachl M, Ramharter J, Savarese F, Gerlach D, Marszalek JR, et al. BI-3406, a potent and selective SOS1-KRAS interaction inhibitor, is effective in KRAS-driven cancers through combined MEK inhibition. Cancer Discov. 2021;11:142–57.
55. Hong SH, Yoo DY, Conway L, Richards-Corke KC, Parker CG, Arora PS. A Sos proteomimetic as a pan-Ras inhibitor. Proc Natl Acad Sci USA. 2021;118: e2101027118.
56. Bery N, Miller A, Rabbitts T. A potent KRAS macromolecule degrader specifically targeting tumours with mutant KRAS. Nat Commun. 2020;11:3233.
57. Lu S, He X, Yang Z, Chai Z, Zhou S, Wang J, et al. Activation pathway of a G protein-coupled receptor uncovers conformational intermediates as targets for allosteric drug design. Nat Commun. 2021;12:4721.
58. Lu S, Chen Y, Wei J, Zhao M, Ni D, He X, et al. Mechanism of allosteric activation of SIRT6 revealed by the action of rationally designed activators. Acta Pharm Sin B. 2021;11:1355–61.
59. Ni D, Wei J, He X, Rehman AU, Li X, Qiu Y, et al. Discovery of cryptic allosteric sites using reversed allosteric communication by a combined computational and experimental strategy. Chem Sci. 2021;12:464–76.
60. Li X, Wang C, Peng T, Chai Z, Ni D, Liu Y, et al. Atomic-scale insights into allosteric inhibition and evolutional rescue mechanism of *Streptococcus thermophilus* Cas9 by the anti-CRISPR protein AcrIIA6. Comput Struct Biotechnol J. 2021;19:6108–24.
61. Feng L, Lu S, Zheng Z, Chen Y, Zhao Y, Song K, et al. Identification of an allosteric hotspot for additive activation of PPARγ in antidiabetic effects. Sci Bull. 2021;66:1559–70.
62. Ah Byun J, VanSchouwen B, Akimoto M, Melacini G. Allosteric inhibition explained through conformational ensembles sampling distinct "mixed" states. Comput Struct Biotechnol J. 2020;18:3803–18.
63. Foutch D, Pham B, Shen T. Protein conformational switch discerned via network centrality properties. Comput Struct Biotechnol J. 2021;19:3599–608.